

Scanning transmission soft x-ray microscopy at beamline X-1A at the NSLS – advances in instrumentation and selected applications

Michael Feser^{*a}, Tobias Beetz^a, Chris Jacobsen^a, Janos Kirz^a, Sue Wirick^a,
Aaron Stein^a, Thorsten Schäfer^{**a,b}
^aSUNY Stony Brook, ^bForschungszentrum Karlsruhe

ABSTRACT

Soft x-ray scanning transmission x-ray microscopy allows one to image dry and wet environmental science, biological, polymer, and geochemical specimens on a nanoscale. Recent advances in instrumentation at the X-1A beamline at the National Synchrotron Light Source at Brookhaven National Laboratory are described. Recent results on Nomarski differential phase contrast and first results of investigations at the oxygen K edge and iron L edge of hydrous ferric oxide transformations are presented.

Keywords: Spectromicroscopy, soft x-ray spectroscopy, scanning transmission x-ray microscopy

1.INTRODUCTION

Scanning transmission x-ray microscopy is used for high resolution imaging, and x-ray absorption spectroscopy of small regions. At Stony Brook, we use the method for a wide range of collaborative studies of environmental and biological systems. In this paper we first outline recent advances in instrumentation at X-1A describing the microscope systems, focusing optics and detector systems. Recent results on Nomarski differential phase contrast in conjunction with a new segmented integrating silicon detector are presented. We also show how spectromicroscopic investigations of hydrous ferric oxide transformations at the oxygen K edge and iron L edge can help in the understanding of actinide mobility in soil samples.

2.MICROSCOPE INSTRUMENTATION

Scanning transmission x-ray microscopes (STXMs) need to be illuminated with spatially coherent light to deliver the full spatial resolution, which is limited by the numerical aperture of the Fresnel zone plate (FZP). A STXM therefore is well suited for use with undulator sources at low-emittance storage rings. The X-ray ring at the National Synchrotron Light Source at Brookhaven National Laboratory has a soft x-ray undulator (X-1) that delivers quasi-monochromatic flux into a few spatial modes vertically, and about a hundred spatial modes horizontally. More than half of the horizontal output of the undulator is being used by a spectroscopy beamline (X-1B). The beamline X-1A has two branch lines delivering about 1 spatial mode to two endstations. The original beamline used one monochromator with two exit slits³, which has been replaced with a new pair of beamlines that have higher energy resolution, and independent monochromators for each microscope endstation⁴. Both endstations can operate simultaneously within the constraint of the undulator spectral output for a particular choice of the undulator gap. A common mode of operation is to choose an undulator gap that allows spectromicroscopic investigations at the Carbon K absorption edge (284 eV) using the undulator fundamental on one endstation, and at the Oxygen K absorption edge (540 eV) using the first harmonic on the other.

2.1. Zone plate optics

Since solid materials are very absorbing for x-ray energies below 1 keV, refractive lenses cannot be used as optical elements. Instead the STXM uses a circular diffraction grating (the FZP) to produce a high

* Michael.Feser@sunysb.edu; phone 1 631 344-4723; fax 1 631 632-8101; <http://www.physics.sunysb.edu>;
Department of Physics & Astronomy, SUNY Stony Brook, Stony Brook, NY, USA 11794-3800

** schaefer@ine.fzk.de; phone 49 7247 82-5494; <http://w3.fzk.de/INE/>; fax 49 7247 82-3927; Institute for Nuclear Waste Management (INE), Forschungszentrum Karlsruhe, PO Box 3640, D-76021 Karlsruhe, Germany

resolution probe. The FZPs used in the microscopes at X-1A are fabricated using electron beam lithography in a collaborative program^{5,6} with Don Tennant of Agere Systems (formerly Lucent Technologies Bell Labs). In the past year a new electron beam lithography system (JEOL JBX-9300FS) has been installed in his lab. Tennant has used this machine to draw 18 nm lines in ZEP 520 photoresist with the 100 keV electron beam, and he has demonstrated that the patterning accuracy is 7 nm (3σ) over a 400 μm writing field. This performance is achieved through the use of dynamic compensation of focus, stigmatism, and placement. Present efforts by A. Stein and M. Lu of Stony Brook are aimed at exploiting this system for fabrication of FZPs for soft x-ray microscopy; optical testing is now underway of FZPs with 160 μm diameter and 30 nm outermost zone width.

2.2. Microscope systems

The X-1A beamline has three STXMs in operation. One of these is a cryoSTXM which is used to study radiation-sensitive specimens at -160°C temperature. At these temperatures radiation induced mass loss is greatly reduced, and plunge freezing in liquid cryogenics such as liquid ethane provides good structural preservation in biological specimens⁸. This system has also been used for demonstrations of tomographic imaging, including a reconstruction of a frozen hydrated fibroblast at approximately $100\times 100\times 250$ nm resolution⁹. Recent studies with the cryoSTXM by T. Beetz of Stony Brook have centered on a more detailed understanding of the effects of temperature on bond damage in near-edge spectroscopy.

Two new room temperature microscopes of identical design have recently entered operation¹⁰. One of these is used primarily for carbon edge imaging and spectroscopy, while the other shares beamtime with the cryoSTXM and is used primarily in the 400-800 eV energy range. These microscopes have zone plate optics and order sorting apertures on kinematic mounts for easy removal and replacement, and an improved piezo stage (PI-731) with low positional noise ($<5\text{nm}$) and significantly better field positioning. No measurable errors have been found during a test with a Michelson interferometer setup. The microscope has a motorized stage for detectors that can hold two x-ray detectors and one visible light microscope, which is used for prealignment of the optical components and sample inspection. This facilitates quick and reproducible interchange of detectors and allows us to use position sensitive detectors, that have to be aligned precisely to the optical axis. The alignment is achieved by scanning the detector with respect to the beam to evaluate its proper position with respect to the FZP.

2.3. Detectors

For photon fluxes below 10^6 photons per second photon counting detectors offer good performance in the energy regime below 1 keV. In collaboration with G. Smith and B. Yu of the Instrumentation Division of Brookhaven National Laboratory (ID-BNL), a low pressure proportional counter has been developed with essentially no electronic noise, and an photon detection efficiency that is limited by the absorption in a 100 nm thick chromium coated silicon nitride entrance window¹¹. This detector is used for C-XANES spectromicroscopy experiments on the STXM.

Imaging modalities such as differential phase contrast¹⁵, dark field imaging²¹⁻²⁴ and Nomarski differential interference contrast¹⁷, which we explain in more detail in section 3, require the use of a spatially configured detector. It is also possible to record the full microdiffraction pattern in the detector plane for each sample position^{25,26} at the cost of increased dataset size and image processing time. In collaboration with P. Rehak and G. DeGeronimo (ID-BNL), and L. Strüder (KETEK GmbH, Germany) and P. Holl (Max-Planck-Institut für extraterrestrische Physik) we have developed a segmented silicon detector (Figure 1) with low noise readout electronics²⁰. This detector operates at room temperature without any entrance window and has a noise equivalent of 8 photons rms for 520 eV and 1ms pixel dwell time in the brightfield mode (sum of inner three segments).

3. NOMARSKI DIFFERENTIAL INTERFERENCE CONTRAST

The motivation for phase contrast imaging in soft x-ray microscopy is the potentially significant reduction in radiation dose necessary to image a specimen compared to absorption contrast^{13,15}. Phase contrast in a full field x-ray microscope has been implemented by G. Schmahl *et al.*¹³ by using a metal phase plate in the back focal plane of the objective. The implementation of a phase contrast scheme on a STXM is not simple, since the number of optical elements has to be kept small, because of their low efficiency. In collaboration with F. Polack (LURE, France) and D. Jeux (Institut d'Optique, France) we have carried out first experiments on X-1A, where we used a differential interferometric STXM setup to detect local phase

slopes of a specimen¹⁷. In this setup a wave profiling grating¹⁸ placed in front of the FZP effectively splits the beam into two interfering wavefronts that are slightly tilted with respect to each other. If the STXM is used with such an illumination, the intensity pattern in the detector plane has the form of an annulus, but superimposed on this is an interference pattern from the two tilted wavefronts, which has a bright fringe in the center (Figure 5a). In the presence of a phase gradient in the sample, the bright fringe will shift up or down within the annulus. We recently carried out new experiments employing the segmented integrating silicon detector²⁰ described in section 2.3. We compute the vertical shift of the bright fringe from the signals of the inner three segments of the detector. Figure 6a shows a bright field (absorption contrast) image of some silica spheres, which is obtained by adding the signal from the inner 3 segments. Figure 6c shows the Nomarski phase contrast image, which can be interpreted as a map of the vertical component of the phase gradient in the sample.

In the same experiment we simultaneously acquired differential interference contrast¹⁵ information, where one measures the shift in the “center of mass” of the illumination intensity as illustrated in Figure 5b. This method offers the advantage of having both the horizontal as well as the vertical components of the phase gradient accessible (Figure 6d,e). Figure 6f shows the computed absolute phase gradient map.

4. SPECTROSCOPIC INVESTIGATION OF HYDROUS FERRIC OXIDE TRANSFORMATIONS

The formation of secondary mineral phases in the near and far field of a nuclear repository site is of paramount importance for the mobility of actinides and therefore a major concern in performance assessment analysis. Iron oxides/-hydroxides are the principal corrosion products of the stainless steel canister material and commonly the dominant sorption surface in the geological host rock formation (grain coatings). During the transformation of the metastable low crystalline precursor phase hydrous ferric oxide (HFO) ($\text{Fe}_2\text{O}_3 \cdot 9\text{H}_2\text{O}$) into the stable counterparts goethite (FeOOH) and/or hematite (Fe_2O_3), actinides and their homologues (lanthanides) can be incorporated into the goethite/hematite structure and therefore change the mobility and bioavailability drastically. As pointed out by Gloter *et al.*¹ the intensity of the O K-edge pre-edge peaks are directly correlated with the amount of Fe-O-Fe bonds and thus can be used to determine quantitatively the Fe lattice substitution by other metal cations. We have acquired near edge absorption spectra of the initial HFO phase and the transformation end products goethite and hematite at the O K edge (Figure 2). Due to its low crystallinity HFO lacks the characteristic pre-edge peaks and splitting A1 and A2, which are attributed to transitions from the O 1s core state to antibonding O 2p states hybridized with Fe 3d orbitals. Problems for quantitative analysis in transformation intermediates arise from the fact that the pre-edge intensities depend on the crystallinity of the sample and on the ratio of Fe^{3+} to the total amount of Fe in reductive environments. Pure synthetic hematite spectra in comparison with Lutetium (homologue for Americium) sorbed onto hematite at pH 8 show no significant effect on the pre-edge features by metal sorption (Figure 3). Additionally measured O K edge spectra of transformation end products with the same Lu concentration ($1 \cdot 10^{-3}$ mol/L) indeed show a substantial decrease in pre-edge peak intensity and therefore clearly indicate Lu incorporation into the secondary phase structure. Furthermore the work was extended to investigations on the Fe L edge to quantify iron oxidation states with high spatial resolution. Reference compound spectra of ferric iron oxides (Fe^{3+} L₃ edge onset at 705.9 eV)¹² in comparison with "San Carlos" olivine (Fe^{2+} L₃ edge onset at 704.6 eV)¹² show that with the current X-1A beamline setup, which is not optimized for investigations at the Fe L₃ edge, the energy resolution (~1eV) is sufficient to quantify iron oxidation states (Figure 4). It is therefore planned in the future to monitor redox-reactions on iron oxides with high spatial resolution at X-1A.

5. CONCLUSION

Soft x-ray spectromicroscopy provides a new set of tools for nanometer scale characterization of chemical heterogeneities. This is being used in environmental science, polymer research, biology, and geochemistry, among other fields. A new segmented integrating silicon detector allows faster data acquisition and the use of additional imaging modes like Nomarski differential interference contrast without the need of major reconfiguration of the experimental setup. Spectroscopic characterization on a nanoscale is available at X-1A in the energy regime from 250 – 800 eV on the same sample area. As an example we presented investigations of hydrous ferric oxide transformations where NEXAFS spectra have been acquired on the same sample at the O K edge and Iron L edge.

ACKNOWLEDGEMENTS

We would like to thank D. Pinelli, R. Ryan, E. Von Achen, and B. Yu of the Instrumentation Division of Brookhaven National Laboratory for their help on detectors. Work supported by the National Science Foundation under grants DBI-9986819 and ECS-0099893.

REFERENCES

1. A. Gloter, *Composition and orientation dependence of the O K and Fe L_{2,3} EELS fine structure in Ca₂(Al_xFe_{1-x})₂O₅*, Physical Reviews **B 61**(4), pp. 2587-2593, 2000
2. Z. Wu, *et al.*, *Characterization of iron oxides by x-ray absorption at the oxygen K edge using a full multiple-scattering approach*, Physical Reviews **B 55**(4), pp. 2570-2577, 1997
3. H. Rarback, *et al.*, *Coherent radiation for x-ray imaging – the soft X-ray undulator and the X-1A beamline at the NSLS*, Journal of X-ray Science and Technology **2**, pp. 274-296, 1990
4. B. Winn, *et al.*, *Illumination for coherent soft X-ray applications: the new X-1A beamline at the NSLS*, Journal of Synchrotron Radiation **7**, pp. 395-404, 2000
5. S. Spector, C. Jacobsen, and D. Tennant, *Process optimization for production of sub-20nm soft x-ray zone plates*, Journal of Vacuum Science and Technology **B 15**(6), pp. 2872-2876, 1997
6. D. Tennant, *et al.*, *Electron beam lithography of Fresnel zone plates using a rectilinear machine and trilayer resists*, in⁷, pp. 601-606
7. W. Meyer-Ilse, T. Warwick, and D. Attwood, eds., *X-ray Microscopy: Proceedings of the Sixth International Conference*, (Melville, NY), American Institute of Physics, 2000
8. J. Maser, *et al.*, *Soft x-ray microscopy with a cryo STXM: I. Instrumentation, imaging, and spectroscopy*, Journal of Microscopy **197**, pp. 68-79, 2000
9. Y. Wang, *et al.*, *Soft x-ray microscopy with a cryo STXM: II. Tomography*, Journal of Microscopy **197**, pp. 80-93, 2000
10. M. Feser, *et al.*, *Instrumentation advances and detector development with the Stony Brook scanning transmission x-ray microscope*, in⁷, pp. 367-372
11. M. Feser, *et al.*, *Applications and instrumentation advances with the Stony Brook scanning transmission x-ray microscope*, SPIE proceedings **3449**, pp. 19-29, 1998
12. L. Garvie, and P.R. Buseck, *Ratios of ferrous to ferric iron from nanometer-sized areas in minerals*, Nature **396**, pp. 667-670 (1998)
13. G. Schmahl, D. Rudolph, and P. Guttman, *Phase contrast x-ray microscopy - experiments at the BESSY storage ring*, in¹⁴, pp. 228-232
14. D. Sayre, M. R. Howells, J. Kirz, and H. Rarback, *X-ray Microscopy II*, Springer series in optical sciences **56**, Springer, Berlin, 1988
15. J.R. Palmer, and G.R. Morrison, *Differential phase contrast imaging in x-ray microscopy*, in¹⁶, pp. 278-280
16. A. Michette, G. Morrison, and C. Buckley, *X-ray microscopy III*, Springer series in optical sciences **67**, Springer Verlag, Berlin, 1992
17. F. Polack, D. Joyeux, *et al.*, *Demonstration of phase contrast in scanning transmission x-ray microscopy: comparison of images obtained at NSLS X-1A with numerical simulations*, in⁷, pp. 573-580
18. D. Joyeux, and F. Polack, *A wavefront profiler as an insertion device for scanning phase contrast microscopy*, in¹⁹, pp. II-201 – II-206
19. J. Thieme, G. Schmahl, E. Umbach, and D. Rudolph, *X-ray microscopy and spectromicroscopy*, Springer Verlag, Berlin, 1998
20. M. Feser, *et al.*, *A novel integrating solid state detector with segmentation for scanning transmission soft x-ray microscopy*, to be published in SPIE proceedings **4499**
21. G.R. Morrison, and M.T. Browne, *Darkfield imaging with the scanning transmission x-ray microscope*, Review of Scientific Instruments **63**, pp. 611-614, 1992
22. H.N. Chapman, C. Jacobsen, and S. Williams, *A characterization of dark-field imaging of colloidal gold labels in a scanning transmission x-ray microscope*, Ultramicroscopy **62**(3), pp. 191-213, 1996
23. H.N. Chapman, *et al.*, *Dark-field x-ray microscopy of immunogold-labeled cells*, Journal of the Microscopy Society of America **2**(2), pp. 53-62, 1996
24. S. Vogt, *et al.*, *Dark field x-ray microscopy: the effects of condenser/detector aperture*, Ultramicroscopy **87**, pp. 25-44, 2001
25. G.R. Morrison, *X-ray imaging with a configured detector*, in²⁷

26. H. Chapman, *Phase-retrieval x-ray microscopy by Wigner-distribution deconvolution*, *Ultramicroscopy* **66**, pp. 153-172, 1996
27. V.V. Aristov, and A.I. Erko, *X-ray microscopy IV*, Chernogolovka, Russia, 1994

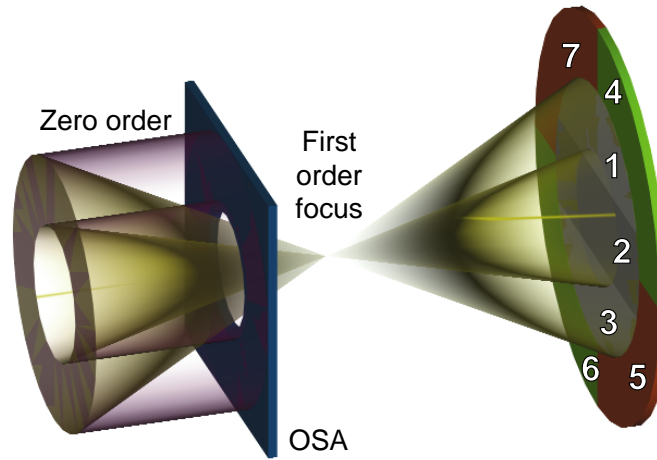


Figure 1: Schematic view of the relationship between the focus of a zone plate in the STXM, and the segmented silicon drift detector. Beam is incident from the left onto the zone plate. The inner three segments (1-3) of the detector are used for bright field detection (sum) and Nomarski differential interference contrast (center of mass). The outer annulus, which is divided in four quadrant segments (4-7) is used for differential interference contrast (center of mass) and dark field contrast (sum; detecting scattered x-rays).

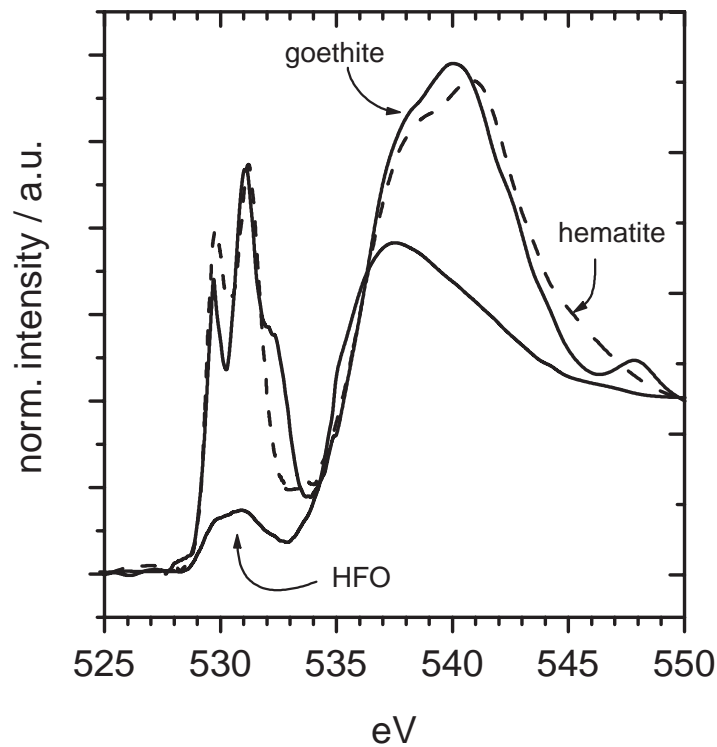


Figure 2: NEXAFS spectra of HFO and its transformation products goethite and hematite.

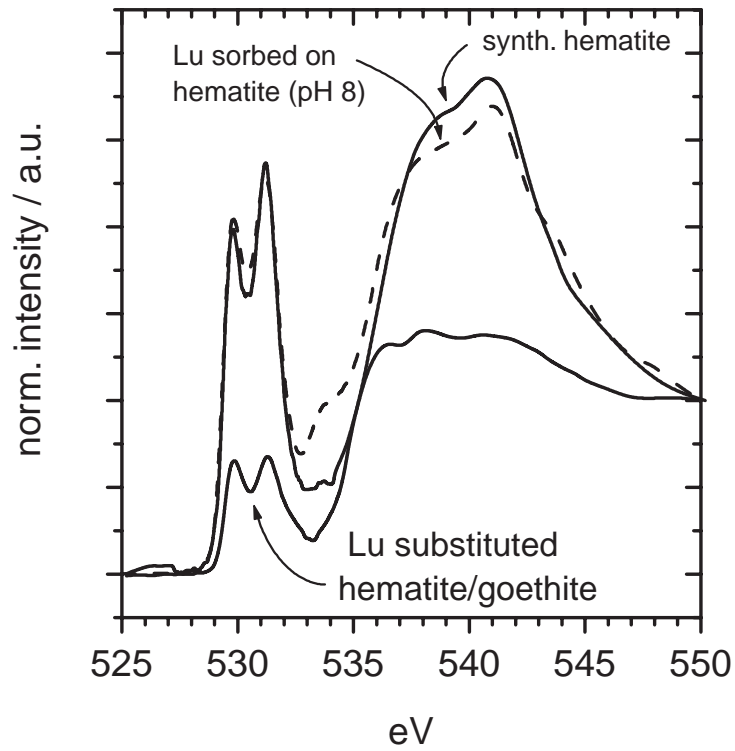


Figure 3: NEXAFS spectra of HFO transformation products in the presence of Lu. A significant decrease in the pre-edge peak intensity is observed which indicates Lu incorporation into the secondary phase structure.

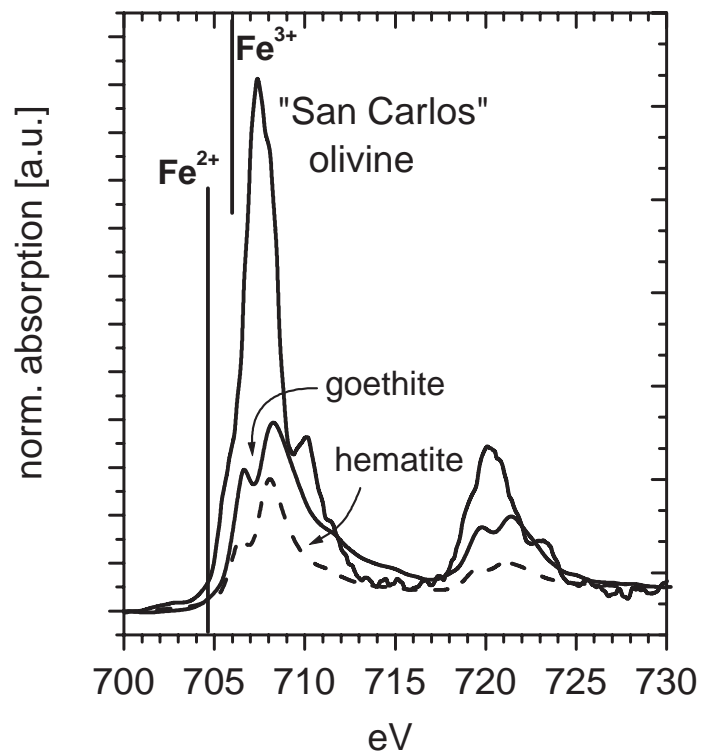


Figure 4: NEXAFS spectra of reference compound spectra to characterize Fe oxidation states.

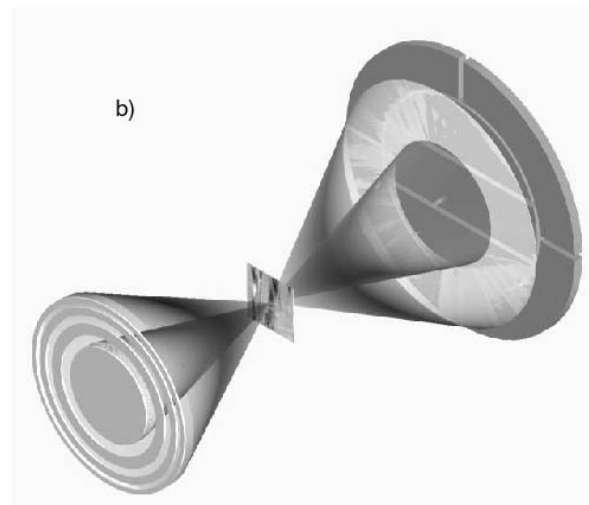
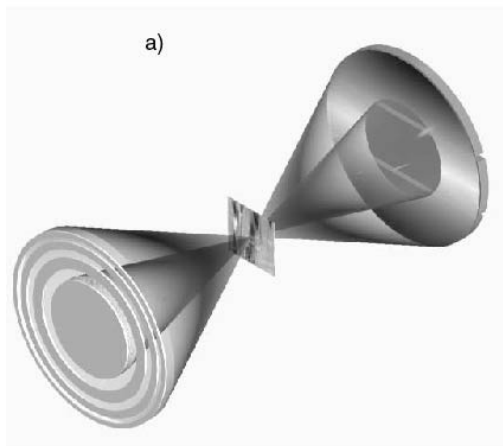


Figure 5: Illustration of differential phase contrast imaging modes.

a.) Nomarski differential interference contrast. X-rays are incident from the left. We are not showing the beamsplitting grating, which is in front of the zone plate. The zone plate focuses the x-rays to a spot through which the sample is raster scanned. On the detector the x-ray intensity distribution is an annulus superimposed by an interference pattern (bright horizontal fringe). The detector consists of 3 segments that monitor shifts of the bright interference fringe in the vertical, which are proportional to the vertical local phase gradient in the specimen.

b.) Differential interference contrast. Four quadrant segments surrounding the inner three segments measure the shift of the “center of mass” of the illumination in the detector plane. The effect is analogous to having a prism in visible light, which refracts the beam.

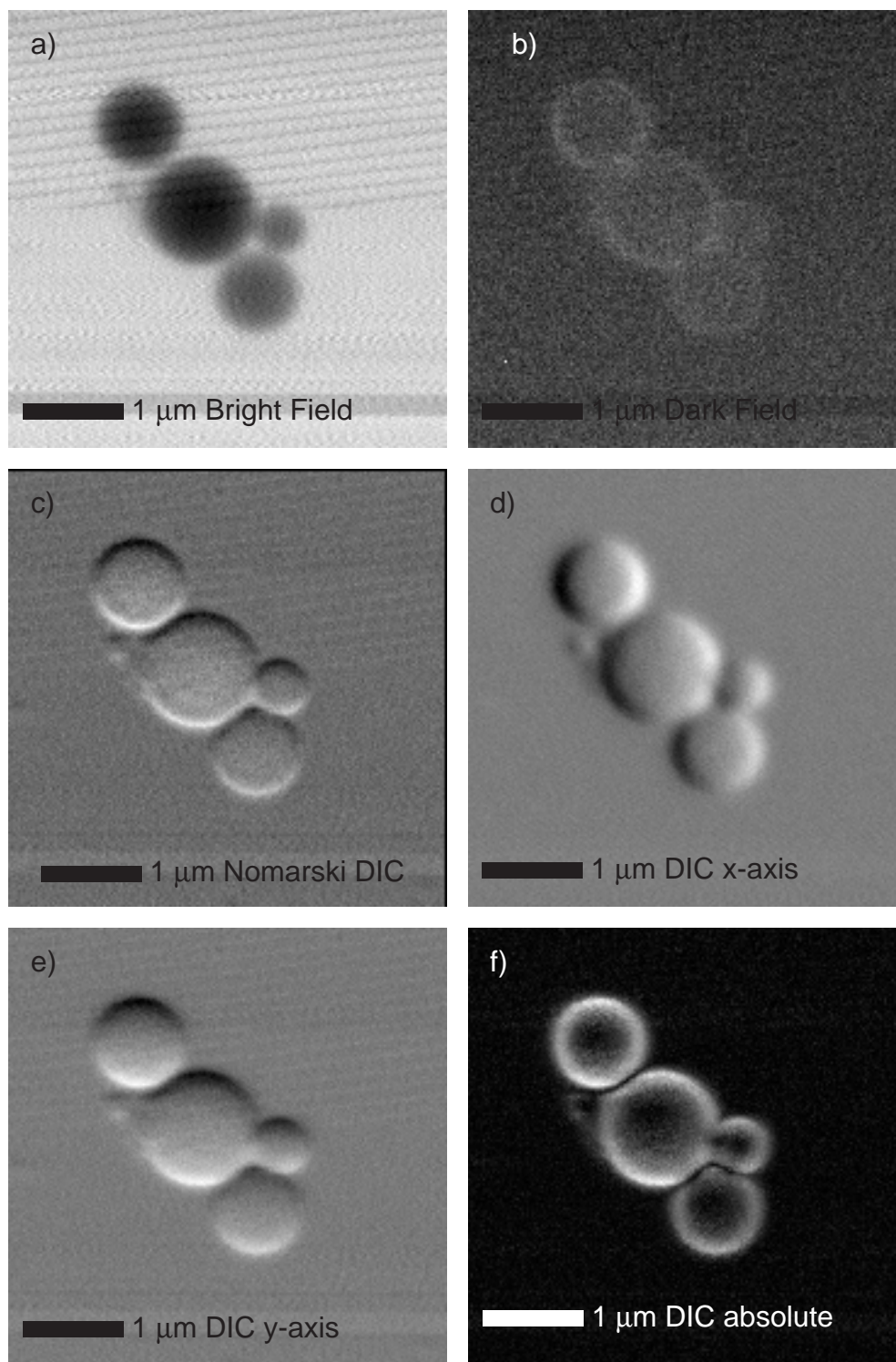


Figure 6: STXM images taken in different imaging modes of silica spheres.

- a) Bright field image (standard imaging mode for spectromicroscopy)**
- b) Dark field image (scattered x-rays only)**
- c) Nomarski differential phase contrast**
- d) Differential interference contrast (center of mass of detected illumination in horizontal direction)**
- e) Differential interference contrast (center of mass of detected illumination in vertical direction)**
- f) Differential interference contrast – absolute of phase gradient**